

Ordered vs Disordered States of the Random-Field Model in Three Dimensions

D. A. Garanin and E. M. Chudnovsky

Physics Department, Lehman College, City University of New York
250 Bedford Park Boulevard West, Bronx, New York 10468-1589, USA

March 1, 2022

Abstract. We report numerical investigation of the glassy behavior of random-field exchange models in three dimensions. Correlation of energy with the magnetization for different numbers of spin components has been studied. There is a profound difference between the models with two and three spin components with respect to the stability of the magnetized state due to the different kinds of singularities: vortex loops and hedgehogs, respectively. Memory effects pertinent to such states have been investigated. Insight into the mechanism of the large-scale disordering is provided by numerically implementing the Imry-Ma argument in which the spins follow the random field averaged over correlated volumes. Thermal stability of the magnetized states is investigated by the Monte Carlo method.

PACS. 74.25.Uv Vortex phases (includes vortex lattices, vortex liquids, and vortex glasses) – 75.10.Nr Spin-glass and other random models – 02.60.Pn Numerical optimization – 64.60.De Statistical mechanics of model systems

1 Introduction

Recently, it has been argued that the behavior of the order parameter in the random field (RF) model described by the Hamiltonian

$$\mathcal{H} = \int d^d r \left[\frac{\alpha_e}{2} (\partial_\mu \mathbf{S}) \cdot (\partial_\mu \mathbf{S}) - \mathbf{h} \cdot \mathbf{S} \right] \quad (1)$$

is controlled by topology. [1] Here α_e is the exchange stiffness and \mathbf{S} is the n -component fixed-length vector field (e.g., spin density of constant length S_0) interacting with the n -component RF $\mathbf{h}(\mathbf{r})$ in d dimensions. Summation over repeated indices is assumed. At $n > d+1$ the behavior of the system is fully reversible with the non-ferromagnetic ground state and exponential decay of spin-spin correlations, while at $n \leq d+1$ the system exhibits glassy behavior with its state determined by the initial condition. [2] In the latter case, the fully ordered initial state relaxes to the partially disordered state possessing a non-zero magnetization that we call the F-state. For the xy model ($n = 2$) in three dimensions the properties of that state have been studied in Ref. [3]. In this paper we focus on the comparative study of the F-state in a $3d$ xy model and in a $3d$ Heisenberg model ($n = 3$) with the goal to shed more light on the glassy properties of the RF system.

The problem has a long history. More than forty years ago Larkin, within a conceptually similar model, argued that randomly positioned pinning centers destroy the translational order in a flux-line lattice. [4] Correlations associated with the translational order in flux lattices are

of practical interest because they define the size of the vortex bundle that gets depinned by the transport current, which, in turn, determines the critical current. [5] Related to this effect is a more general qualitative argument suggested by Imry and Ma. [6] It states that a static RF, regardless of strength, destroys the long-range order associated with a continuous-symmetry order parameter below $d = 4$ spatial dimensions. Aizenman and Wehr [7, 8] provided a mathematical argument that is considered to be a rigorous proof of the Imry-Ma statement. According to this statement the directions of \mathbf{S} are correlated only within randomly oriented domains of average size $R_f \propto (1/h)^{2/(4-d)}$. Same R_f comes from the Green-function method. [9] These ideas have been applied to random magnets, [10, 11, 12, 14] disordered antiferromagnets, [15] spin-glasses, [16] arrays of magnetic bubbles, [17] superconductors, [18, 5] charge-density waves, [19] liquid crystals, [20] superconductor-insulator transition, [21] and superfluid $^3\text{He-A}$ in aerogels. [22, 23]

In early 1980s the renormalization group treatments of the problem by Cardy and Ostlund [24] and by Villain and Fernandez [25] questioned the validity of Larkin-Imry-Ma (LIM) argument for distances $R \gtrsim R_f$. The application of scaling and replica-symmetry breaking arguments to statistical mechanics of flux lattices, [26, 27, 28, 29, 30, 31, 32, 33, 34, 35, 36] as well as the variational approach, [37, 38] yielded the power-law decay of correlations at large distances. These findings suggested that ordering could be more robust against weak static randomness than expected from the LIM theory. Such a quasicrystalline

phase, presumed to be vortex-free in spin systems and dislocation-free in flux lattices, received the name of a Bragg glass. Fisher [39] called it an “elastic glass” and argued that the energy associated with vortex loops prevents the xy 3d RF system from complete disordering.

Numerical evidence of the Bragg/elastic glass has been inconclusive so far. Early numerical work on 1d (Ref. [40]) and 2d (Ref. [41]) spin systems with quenched random anisotropy established strong non-equilibrium effects, such as magnetic hysteresis and dependence on the initial conditions. Defect-free spin models with relatively large RF and random anisotropy have been studied numerically on small lattices by Fisch. [42] In three dimensions strong non-equilibrium effects have been reported in Refs. [43, 2, 3]. Numerical studies of the 2d elastic media with pinning centers (that is similar to 2d xy model) [44] revealed that pinning creates dislocations and thus destroys the Bragg glass. In line with the conjecture made in Ref. [39], it was suggested in Ref. [3] that the high energy cost of vortex loops was preventing the spins in the xy 3d RF model from relaxing to a disordered state from the initially ordered state. At elevated temperatures, however, the numerical evidence of the power-law decay of correlations in a 2d random-field xy model has been recently obtained by Perret et al. [45] In the absence of topological defects, the evidence of the logarithmic growth of misalignment with the size of the system has been also found in 2d Monte Carlo studies of a crystal layer on a disordered substrate and for pinned flux lattices. [46, 47] The power-law decay of spin-spin correlations has been reported in Monte Carlo studies of the RF Heisenberg model, [48] as well as for the xy model. [49] As to the real experiments, large areas of defect-free flux lattices have been reported in Ref. [50]. The comparison of such experiments with theory is hampered, however, by the fact that for a weak disorder the correlation length in 3d can be very large, making it difficult to distinguish large defect-free slightly disordered domains from the Bragg glass.

The paper has the following structure. Some rigorous analytical results that serve as the test for numerics are given in Section 2. Numerical method and the model used in computations are specified in Section 3. Energy of the F-state as a function of the magnetization for different number of spin components is obtained in Section 4. Evolution of the F-state generated by a hysteresis cycle is studied in Section 5. The dependence of the magnetization of the F-state as function of the strength of the RF is reported in Section 6. Numerical implementation of the Imry-Ma argument is developed in Section 7. Microscopic structure of the F-state is discussed in Section 8. Memory of the initial condition that results in the rotational elasticity of the F-state is demonstrated in Section 9. Section 10 deals with the effect of finite temperature on the F-state. Our conclusions are given in Section 11.

2 Analytical Results

The discrete counterpart of the Hamiltonian (1) that takes into account the Zeeman interaction of spins with the ex-

ternal field \mathbf{H} is given by

$$\mathcal{H} = -\frac{1}{2} \sum_{ij} J_{ij} \mathbf{s}_i \cdot \mathbf{s}_j - \sum_i \mathbf{h}_i \cdot \mathbf{s}_i - \mathbf{H} \cdot \sum_i \mathbf{s}_i, \quad (2)$$

where \mathbf{s}_i is a n -component constant-length ($|\mathbf{s}_i| = s$) spin at the site i of a cubic lattice and \mathbf{h}_i is a quenched RF at that site. The summation is over the nearest neighbors. The factor $1/2$ in the first term is compensating for the double counting of the exchange bonds. In what follows we assume nearest-neighbor exchange. The connection between the parameters of the continuous and discrete models is $\alpha_e = Ja^{d+2}$ and $S_0 = s/a^d$, with a being the lattice spacing. Eq. (2) contains the exchange energy per spin of the collinear state, $E_0 = -3Js^2$, that is not included in Eq. (1).

In this paper we present numerical results on the energy minimization in Eq. (2) for the uncorrelated RF,

$$\langle h_{i\alpha} h_{j\beta} \rangle = \frac{h^2}{n} \delta_{\alpha\beta} \delta_{ij}, \quad (3)$$

(Greek indices being the Cartesian components of the vectors) although computations for a correlated RF have been performed as well. Our main choice for the numerical work has been a fixed-length RF: $|\mathbf{h}_i| = h = \text{const}$. No difference has been found for models with a distributed RF strength, e.g. Gaussian.

Before doing numerical work it is useful to obtain some exact analytical formulas that can provide the ultimate test for our numerical results. One such formula describes the short-range behavior of spin-spin correlations. Choosing in 3d

$$\mathcal{H}_\lambda = \mathcal{H} - \int d^3r \lambda(\mathbf{r}) \mathbf{S}^2 \quad (4)$$

to account for $\mathbf{S}^2 = S_0^2 = \text{const}$ by the term containing a Lagrange multiplier $\lambda(\mathbf{r})$, one obtains the following extremal equation for \mathbf{S} :

$$\alpha_e \nabla^2 \mathbf{S} + \mathbf{h} + 2\lambda \mathbf{S} = 0. \quad (5)$$

Multiplying this by \mathbf{S} we have

$$\lambda = -\frac{1}{2S^2} (\alpha_e \mathbf{S} \cdot \nabla^2 \mathbf{S} + \mathbf{S} \cdot \mathbf{h}) \quad (6)$$

$$\alpha_e \nabla^2 \mathbf{S} - \frac{\alpha_e}{S_0^2} \mathbf{S} (\mathbf{S} \cdot \nabla^2 \mathbf{S}) + \mathbf{h} - \frac{1}{S_0^2} \mathbf{S} (\mathbf{S} \cdot \mathbf{h}) = 0. \quad (7)$$

In the second term of Eq. (7)

$$\mathbf{S} \cdot \nabla^2 \mathbf{S} = \partial_\mu (\mathbf{S} \cdot \partial_\mu \mathbf{S}) - \partial_\mu \mathbf{S} \cdot \partial_\mu \mathbf{S} = -\partial_\mu \mathbf{S} \cdot \partial_\mu \mathbf{S} \quad (8)$$

because

$$\mathbf{S} \cdot \partial_\mu \mathbf{S} = \frac{1}{2} \partial_\mu S^2 = 0. \quad (9)$$

As long as small volumes are concerned, this term is quadratic on the perturbation of \mathbf{S} caused by the weak RF and, therefore, it is small compared to other terms in Eq. (7) that are linear on \mathbf{h} . Consequently, at small distances this

term can be safely dropped. Implicit solution of the remaining equation is

$$\mathbf{S}(\mathbf{r}) = -\frac{1}{\alpha_e} \int d^3r' G(\mathbf{r}-\mathbf{r}') \left\{ \mathbf{h}(\mathbf{r}') - \frac{\mathbf{S}(\mathbf{r}')[\mathbf{S}(\mathbf{r}') \cdot \mathbf{h}(\mathbf{r}')] }{S_0^2} \right\} \quad (10)$$

with $G(\mathbf{r}) = -1/(4\pi|\mathbf{r}|)$ being the Green function of the 3d Laplace equation. Then

$$\begin{aligned} & \frac{1}{2S_0^2} \langle [\mathbf{S}(\mathbf{r}_1) - \mathbf{S}(\mathbf{r}_2)]^2 \rangle = \\ & = \frac{1}{2\alpha_e^2 S_0^2} \int d^3r' \int d^3r'' [G(\mathbf{r}_1 - \mathbf{r}') - G(\mathbf{r}_2 - \mathbf{r}')] \times \\ & [G(\mathbf{r}_1 - \mathbf{r}'') - G(\mathbf{r}_2 - \mathbf{r}'')] \langle \mathbf{g}(\mathbf{r}') \cdot \mathbf{g}(\mathbf{r}'') \rangle, \end{aligned} \quad (11)$$

where $\mathbf{g} \equiv \mathbf{h} - \mathbf{S}(\mathbf{S} \cdot \mathbf{h})/S_0^2$.

Neglecting the weak correlation between \mathbf{h} and \mathbf{S} , with the help of the continuous equivalent of Eq. (3),

$$\langle h_\alpha(\mathbf{r}') h_\beta(\mathbf{r}'') \rangle = \frac{h^2}{n} \delta_{\alpha\beta} a^3 \delta(\mathbf{r}' - \mathbf{r}''), \quad (12)$$

one obtains

$$\langle g_\alpha(\mathbf{r}') g_\beta(\mathbf{r}'') \rangle = \frac{h^2}{n} \left(\delta_{\alpha\beta} - \frac{\langle S_\alpha S_\beta \rangle}{S_0^2} \right) a^3 \delta(\mathbf{r}' - \mathbf{r}''). \quad (13)$$

Consequently

$$\langle \mathbf{g}(\mathbf{r}') \cdot \mathbf{g}(\mathbf{r}'') \rangle = \frac{h^2}{n} (n-1) a^3 \delta(\mathbf{r}' - \mathbf{r}''). \quad (14)$$

This gives

$$\begin{aligned} & \frac{1}{2S_0^2} \langle [\mathbf{S}(\mathbf{r}_1) - \mathbf{S}(\mathbf{r}_2)]^2 \rangle = \\ & = \frac{h^2 a^3}{2\alpha_e^2 S_0^2} \left(1 - \frac{1}{n} \right) \int d^3r [G(\mathbf{r}_1 - \mathbf{r}) - G(\mathbf{r}_2 - \mathbf{r})]^2 \\ & = \frac{h^2 a^3}{8\pi\alpha_e^2 S_0^2} \left(1 - \frac{1}{n} \right) |\mathbf{r}_1 - \mathbf{r}_2| = \frac{|\mathbf{r}_1 - \mathbf{r}_2|}{R_f} \end{aligned} \quad (15)$$

with [1]

$$\frac{R_f}{a} = \frac{8\pi\alpha_e^2 S_0^2}{h^2 a^4 (1-1/n)} = \frac{8\pi}{(1-1/n)} \left(\frac{Js}{h} \right)^2. \quad (16)$$

The weakness of the RF should be measured against the exchange field $6Js$ created in a 3d cubic lattice by the nearest neighbors of each spin. This can be seen by presenting Eq. (16) in the form

$$\frac{R_f}{a} = \frac{2\pi}{9(1-1/n)} \left(\frac{6Js}{h} \right)^2, \quad (17)$$

with the numerical factor in front of $(6Js/h)^2$ of order unity, e.g., $2\pi/6$ for $n=3$.

Noticing that

$$\frac{1}{2S_0^2} \langle [\mathbf{S}(\mathbf{r}_1) - \mathbf{S}(\mathbf{r}_2)]^2 \rangle = 1 - \frac{1}{S_0^2} \langle \mathbf{S}(\mathbf{r}_1) \cdot \mathbf{S}(\mathbf{r}_2) \rangle \quad (18)$$

we finally obtain

$$\langle \mathbf{s}_i \cdot \mathbf{s}_j \rangle = s^2 \left(1 - \frac{|\mathbf{r}_i - \mathbf{r}_j|}{R_f} \right). \quad (19)$$

This formula is in agreement with the famous Larkin's result, [4] with Eq. (16) providing the correlation length for arbitrary n .

Long-range correlations are difficult to obtain by the above Green-function method because of the high non-linearity of Eq. (7). However, the case of $n = \infty$ permits an exact analytical solution at all distances due to its equivalence [51] to the mean-spherical model in which only the volume average of \mathbf{S}^2 rather than the local \mathbf{S}^2 is a constant, $V^{-1} \int d^3r \mathbf{S}^2 = S_0^2$. In this case λ in Eq. (5) is a constant that we will write as $\lambda = -\alpha_e k^2/2$. Then the extremal equation for \mathbf{S} is linear

$$(\nabla^2 - k^2) \mathbf{S} = -\frac{1}{\alpha_e} \mathbf{h} \quad (20)$$

with a general solution

$$\mathbf{S}(\mathbf{r}) = -\frac{1}{\alpha_e} \int d^3r' G_k(\mathbf{r} - \mathbf{r}') \mathbf{h}(\mathbf{r}'), \quad (21)$$

$G_k(\mathbf{r}) = -e^{-k|\mathbf{r}|}/(4\pi|\mathbf{r}|)$ and $G_k(\mathbf{q}) = -1/(q^2 + k^2)$ being the Green function of Eq. (20) and its Fourier transform, respectively. Consequently,

$$\begin{aligned} \langle \mathbf{S}(\mathbf{r}_1) \cdot \mathbf{S}(\mathbf{r}_2) \rangle &= \frac{1}{\alpha_e^2} \int d^3r d^3r' G_k(\mathbf{r}_1 - \mathbf{r}') G_k(\mathbf{r}_2 - \mathbf{r}'') \\ &\times \langle \mathbf{h}(\mathbf{r}') \cdot \mathbf{h}(\mathbf{r}'') \rangle = \frac{h^2 a^3}{\alpha_e^2} \int d^3r G_k(\mathbf{r} - \mathbf{r}_1) G_k(\mathbf{r} - \mathbf{r}_2) \\ &= \frac{h^2 a^3}{\alpha_e^2} \int \frac{d^3q}{(2\pi)^3} \frac{e^{i\mathbf{q} \cdot (\mathbf{r}_1 - \mathbf{r}_2)}}{(q^2 + k^2)^2} = \frac{h^2 a^3}{8\pi\alpha_e^2 k} e^{-k|\mathbf{r}_1 - \mathbf{r}_2|}. \end{aligned} \quad (22)$$

Writing the correlation function in the form $\langle \mathbf{S}(\mathbf{r}_1) \cdot \mathbf{S}(\mathbf{r}_2) \rangle = S_0^2 \exp(-|\mathbf{r}_1 - \mathbf{r}_2|/R_f)$, we finally obtain $k = 1/R_f$,

$$\langle \mathbf{s}_i \cdot \mathbf{s}_j \rangle = s^2 \exp \left(-\frac{|\mathbf{r}_i - \mathbf{r}_j|}{R_f} \right) \quad (23)$$

where

$$\frac{R_f}{a} = \frac{8\pi\alpha_e^2 S_0^2}{h^2 a^4} = 8\pi \left(\frac{Js}{h} \right)^2. \quad (24)$$

This result is in agreement with Eqs. (16) and (19) at $n = \infty$.

Two effects contribute to the energy associated with the disorder. The first, that we call the short-range (SR) energy, is associated with local disturbance of the ferromagnetic order by the RF. It does not depend on the large-scale rotation of the magnetization characterized by $R_f \gg a$. The second, that we call the long-range (LR) energy, is associated with that large-scale rotation. Substituting Eq. (21) into Eq. (1) and integrating by parts we obtain

$$\begin{aligned} \mathcal{H} &= -\frac{1}{2\alpha_e} \int d^3r d^3r' d^3r'' G_k(\mathbf{r} - \mathbf{r}') \nabla_r^2 G_k(\mathbf{r} - \mathbf{r}'') \\ &\times \mathbf{h}(\mathbf{r}') \cdot \mathbf{h}(\mathbf{r}'') + \frac{1}{\alpha_e} \int d^3r d^3r' G_k(\mathbf{r} - \mathbf{r}') \mathbf{h}(\mathbf{r}) \cdot \mathbf{h}(\mathbf{r}'). \end{aligned} \quad (25)$$

Here the first term originates from the exchange interaction and the second term originates from the interaction of \mathbf{S} with the RF. Averaging this expression with the help of Eq. (12) gives for the energy density

$$\frac{\langle \mathcal{H} \rangle}{V} = \frac{h^2 a^3}{\alpha_e} \int d^3 r \left[-\frac{1}{2} G_k(\mathbf{r}) \nabla^2 G_k(\mathbf{r}) + G_k(\mathbf{r}) \delta(\mathbf{r}) \right] \quad (26)$$

Recalling that $(\nabla^2 - k^2)G_k(\mathbf{r}) = \delta(\mathbf{r})$, for the energy per spin $E = (\langle \mathcal{H} \rangle / V) a^3$ one obtains

$$E = \frac{h^2 a^6}{\alpha_e} \int d^3 r \left[-\frac{k^2}{2} G_k^2(\mathbf{r}) + \frac{1}{2} G_k(\mathbf{r}) \delta(\mathbf{r}) \right]. \quad (27)$$

Computation of the first term in Eq. (27) involves integration over distances of order R_f . It gives the long-range (LR) energy of the mean spherical model ($n \rightarrow \infty$):

$$E_{\text{LR}} = -\frac{h^4}{128\pi^2 J^3 s^2}. \quad (28)$$

The last negative ($G_k < 0$) term in Eq. (27) that contains the δ -function is the combined short-range (SR) exchange and RF energy, the RF energy being negative and twice the exchange energy, both proportional to h^2 . These integrals formally diverge because of the singularity of $G_k(r)$ at $r = 0$, which is an artifact of the continuous field theory. They can be estimated by replacing G_k with $1/a$ at $r \rightarrow 0$. It is possible, however, to compute the SR energy approximately for the general n -component model by using the discrete Hamiltonian, Eq. (2) and the relation between the exchange energy and the nearest-neighbor spin correlation function. Subtracting the energy $E_0 = -3Js^2$, of the ferromagnetically ordered state, one obtains for the SR exchange energy per spin

$$E_{\text{SR},ex} = 3J[s^2 - \langle \mathbf{s}(0) \cdot \mathbf{s}(a) \rangle] = \frac{3Js^2 a}{R_f} = \left(1 - \frac{1}{n}\right) \frac{3h^2}{8\pi J}, \quad (29)$$

where Eqs. (19) and (16) have been used. According to the comment below Eq. (28), the total SR energy is

$$E_{\text{SR}} = -\left(1 - \frac{1}{n}\right) \frac{3h^2}{8\pi J}. \quad (30)$$

3 Numerical method

Random-field systems exhibit glassy behavior with many local energy minima. Same as in Ref. [3], at $T = 0$ we minimize the energy of the system in the process of the relaxation from a typical initial state such as, e.g., random or collinear orientation of spins. The method consists of the sequential rotation of each spin towards the direction of the effective field at a given site with the probability α or its flipping over the effective field (the so-called over-relaxation, conserving the energy) with the probability $1 - \alpha$. Computation based upon rotations only had been developed for random-anisotropy systems in Ref. [41]. The addition of the flipping (the so-called over-relaxation) that

conserves energy makes the method more effective. The parameter α has the meaning of the relaxation constant. For our glassy systems the method works most efficiently when small α is used. Most of the results have been obtained with $\alpha = 0.03$. The resulting energy minima are representative local energy minima. No attempt has been made to find the global energy minimum as it would be hopeless for the glassy system of a large size that we have studied. In the physical applications, high energy barriers prevent the glassy system from reaching the global energy minimum.

At nonzero temperatures we use Monte Carlo method described in Sec. 10.1.

In the numerical work we consider a simple cubic lattice with periodic boundary conditions and set $s = a = J = 1$, using H_R instead of h . The numerical method has been implemented in Wolfram Mathematica in a compiled and parallelized form. To reduce statistical fluctuations in our random system, one can do averaging over realizations of the RF. For systems of large sizes that we use the self-averaging over the system produces the same effect. To avoid large fluctuations the system size L must satisfy $R_f \ll L$. For the weak random field, Eq. (16) gives large R_f so that a large L is needed to prove ordering or disordering. For $R_f \gtrsim L$ the system has a large finite-size magnetization in all cases.

Vorticity in the xy model can be computed by considering rotations of spins when one circles the lattice site in the positive direction (counterclockwise) around each square plaquette within xy , yz , and zx planes. [43,3]. If the spins rotate by a zero angle, there is no singularity. Rotation by $\pm 2\pi$ corresponds to the vortex/antivortex. For models with arbitrary number of spin components for each cube of neighboring spins the average spin vector and its length can be computed. If the latter is smaller than a preset value (we used 0.5), there is a singularity at this point. In particular, in the $3d$ Heisenberg model there are so-called hedgehogs, singularity points around which the magnetization points towards the center or away from the center. The proposed method reliably provides positions of hedgehogs in the lattice. The fraction of positions having singularities is reported as f_S . This method works well for any dimensionality of space d and any number of spin components n . For the xy model it yields the results consistent with those obtained by looking for vortices/antivortices.

4 Energy and magnetization

Correlation of the energy of local energy minima with the magnetization in the xy model has been studied in Ref. [3]. The energy of the vortex-glass (VG) state was found to correlate perfectly with the vorticity and to be higher than the energy of the F-state. The latter had a flat minimum at m between 0.5 and 0.6 for $H_R/J = 1.5$. The F-states with lower magnetization (the lowest being just below $m = 0.2$) have manifestly higher energies.

Here a different computation has been performed for models with different n . The energy was minimized under the constraint of $m_z = \text{const}$ applying a self-adjusting field

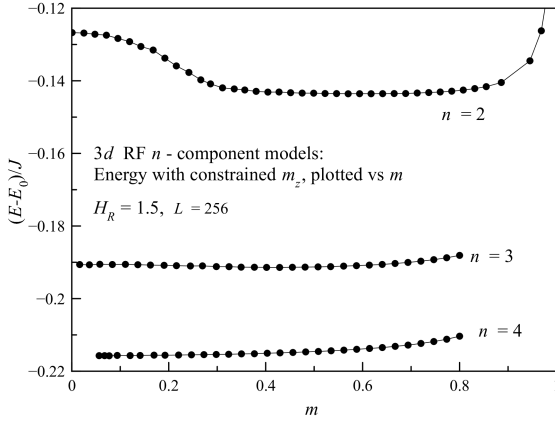


Fig. 1. Energy E vs the magnetization m for different numbers of spin components, $n = 2, 3, 4$. Each point was obtained by relaxation from a random initial state.

H along the z axis as a Lagrange multiplier. We measure energy with respect to the exchange energy, E_0 , of the collinear ferromagnetic state. The resulting difference, $E - E_0$, (without the Lagrange Zeeman energy) was plotted vs resulting magnetization m . Although in the computations the target value of m_z was fixed, other components of \mathbf{m} were not, so that their non-zero values contributed to m . The initial state for the relaxation was random or collinear orientation of spins. The results for different n and random initial conditions are shown in Fig. 1, while the results for different models separately are shown in a finer scale in Fig. 2. The curve $E(m)$ for the xy model ($n = 2$) has a pronounced flat minimum. Higher energy for $m \lesssim 0.2$ is mainly due to vortex loops. Higher energies for m close to 1 are due to the near-collinearity of spins and their non-aligning with the random field.

The curves for $n = 3, 4$ are nearly flat in Fig. 1. However, one can see a minimum of the energy at a finite m for the Heisenberg model ($n = 3$) in the middle panel of Fig. 2. The latter occurs due to hedgehogs in the region of small m that inevitably occur due to topology [1]. Their energy is much smaller than the energy of vortex loops in the xy model, thus the energy minimum is shallow relative to the xy model. The effect of hedgehogs is subtle. In Sec. 5 it will be shown that a more sophisticated method of finding the energy minimum with the help of hysteresis loops with the amplitude of the magnetic field gradually decreasing to zero allows the system to better adjust and attain the minimal-energy state with $m = 0$ in spite of hedgehogs.

For $n = 4$ there are no singularities [1], and the position of the energy minimum can be projected to $m = 0$. Fig. 2 shows all three curves separately. One can see the energy minimum slightly above $m = 0.4$ for the Heisenberg model, $n = 3$.

The presence or absence of singularities in the completely disordered states of the random-field model follow from the topological argument of Ref. [1]. As pointed out by Imry and Ma [6], in the completely disordered state the

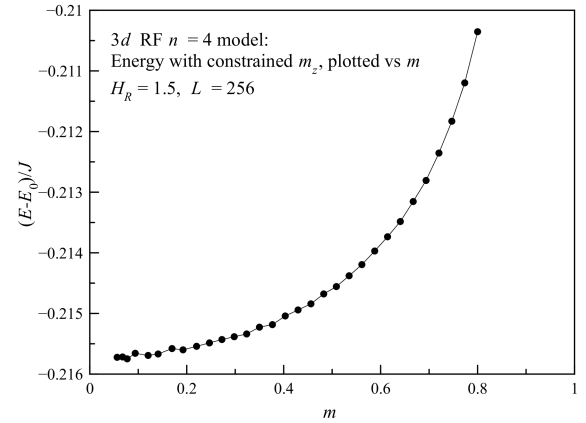
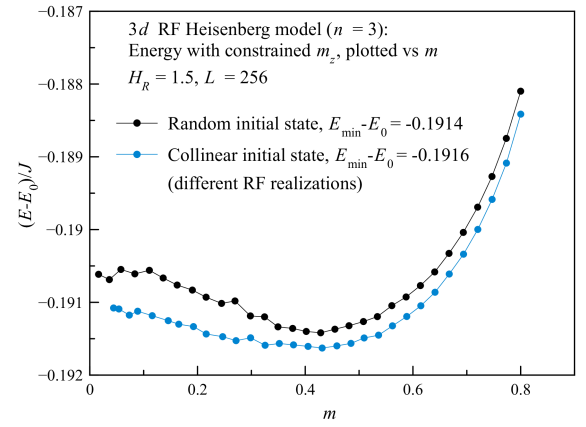
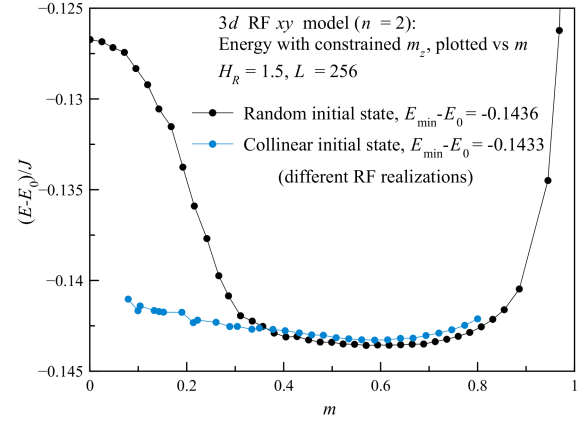


Fig. 2. Energy E vs the magnetization m for different models. Each point was obtained by relaxation from a random or collinear initial state. Note that here the energy scale is finer than in Fig. 1.

magnetization should follow the direction of the random field averaged over large areas $\bar{\mathbf{h}}$. Different components of the average random field \bar{h}_β , $\beta = 1, \dots, n$ are statistically independent and take different signs. Equations $\bar{h}_\beta = 0$, $\beta = 1, \dots, n$ define n surfaces of dimension $d - 1$ in the d -dimensional space of the system. For $n \leq d$ there are subspaces where $\bar{\mathbf{h}} = \mathbf{0}$ and the direction of the magnetization is undefined. Crossing these subspaces cause the

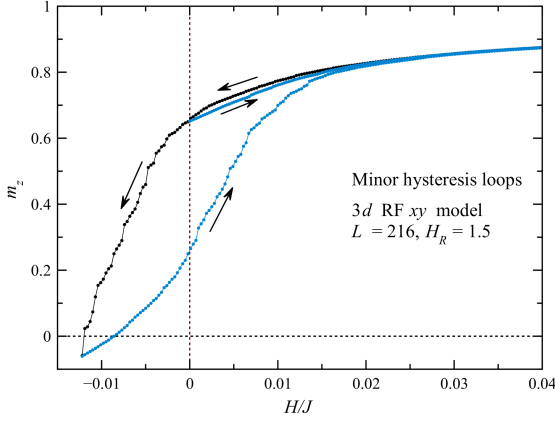


Fig. 3. Minor hysteresis loops in the 3d xy model. All these states are vortex-free.

magnetization vector to abruptly change its direction [1], that is, the subspaces $\mathbf{h} = \mathbf{0}$ correspond to singularities in the spin field.

5 Evolution of the F-state during the hysteresis cycle

The hysteresis loop in the 3d xy model is rather wide because of the formation of topologically stable 180° “spin walls” as the field changes its direction. In spin walls spins are still directed in the old direction, whereas everywhere else the direction of spins follow that of the field (see Sec. “Hysteresis loops” of Ref. [41] and Sec. 5H of Ref. [3]). Spin walls rupture at a particular negative field, creating vortex loops. [3] In the 3d Heisenberg model the hysteresis loop is apparently due to hedgehogs and is much narrower, while the hysteresis loop for the non-singular model with $n = 4$ it almost invisible. [1]

Here we show that the glassy properties of the RF models are not exclusively due to the singularities and that barriers also exist in the vortex-free states of the xy model, leading to minor hysteresis loops. Such loops are shown in Fig. 3. Making repeated hysteresis loops with the amplitude of the applied field H decreasing to zero, one can hope to end up in a state of a smaller energy. To save the computation time, the process can be started as free relaxation in zero field from a collinear state aligned with the direction in which H will be applied. This results in the F-state. Then the field is increased in the direction opposite to the initial magnetization etc. For the 3d xy model, starting with a large m leads to the rupture of spin walls and creation of the vortex loops. As the result, the system ends up in a state of a higher energy than the initial F-state.

For the 3d xy model one can lower the energy of the initial F-state by making hysteresis loops with the initial amplitude smaller than the magnetic field that causes rupture of spin walls. The evolution of the magnetization in this sequence vs the applied field is shown in Fig. 4. Evolution

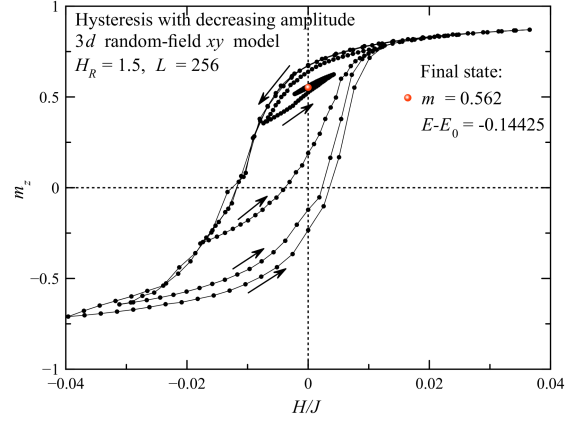


Fig. 4. Evolution of the magnetization in the 3d xy model during the hysteresis cycle with amplitude decreasing to zero, starting from positive fields. All states are vortex free. Using larger initial amplitudes of the magnetic field leads to rupture of spin walls at negative fields and thus creating vortex loops that increase the energy of the system.

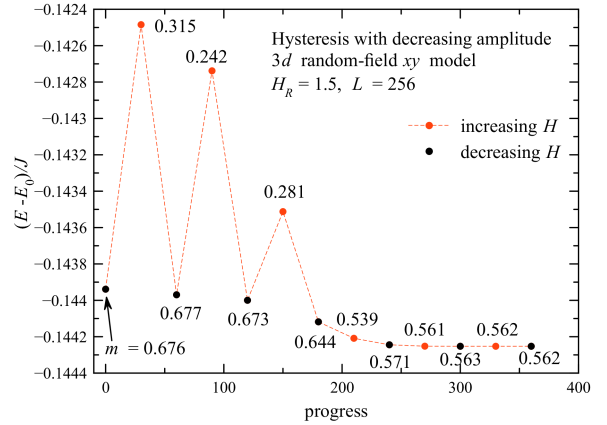


Fig. 5. Evolution of energy in the 3d xy model during the hysteresis cycle with decreasing amplitude. Only points corresponding to $H = 0$ are shown. Black (red) circles correspond to decreasing (increasing) H .

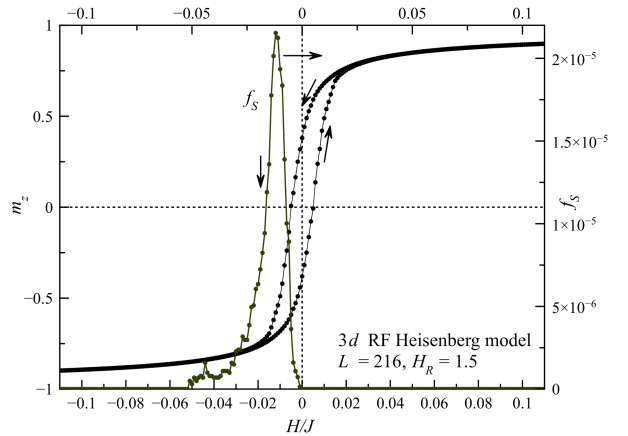


Fig. 6. Hysteresis loop of the 3d Heisenberg model.

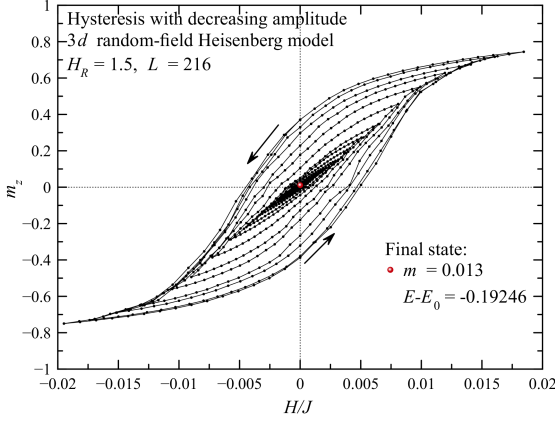


Fig. 7. Evolution of the magnetization in the 3d Heisenberg model during the hysteresis cycle with amplitude decreasing to zero.

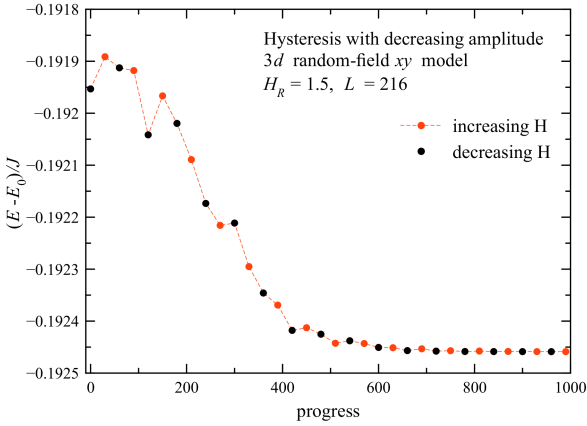


Fig. 8. Evolution of energy in the 3d Heisenberg model during the hysteresis cycle with decreasing amplitude. Only points corresponding to $H = 0$ are shown. Black (red) circle correspond to the decreasing (increasing) H .

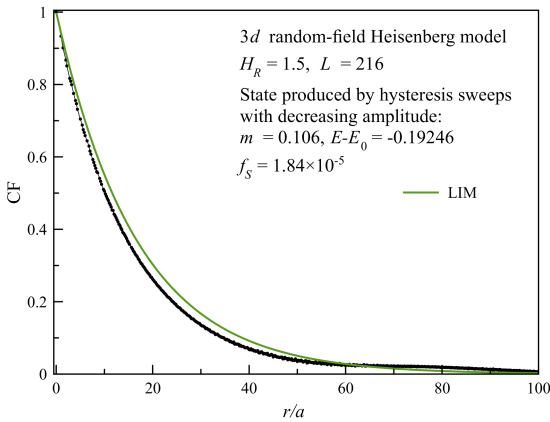


Fig. 9. Spin-spin correlation function of the 3d Heisenberg model at the end of the hysteresis cycle with decreasing amplitude.

of the energy is shown in Fig. 5 (zero values of H only). One can see that the final energy is indeed lower than the initial energy $(E - E_0)/J = -0.1439$ of the state with $m = 0.676$ obtained by relaxation from the collinear state (the first point in Fig. 5). For $H_R/J = 1.5$ and $L = 256$ the final state has $m = 0.562$ and $(E - E_0)/J = -0.14425$. Another computation with $H_R/J = 1.5$ and $L = 216$ resulted in $m = 0.567$ and $(E - E_0)/J = -0.1441$. It is important to notice that the amplitude of the hysteresis loop remains small enough so that rupture of spin walls accompanied by the creation of vortex loops [3] does not occur. Otherwise the process would lead to the energy increase: the final state (also having the large magnetization typical for the F-state) contains singularities and its energy is higher than that of the F-state obtained by relaxation from the collinear state. These experiments show that the F-state of the 3d xy model is robust. It cannot be easily destroyed by manipulating the external field.

A completely different behavior has been observed for the 3d Heisenberg model. Here, as shown in Fig. 7, decreasing the magnetic field to negative values immediately leads to the formation of singularities - hedgehogs. Thus hedgehogs are unavoidable and one can start with a greater amplitude of the field sweep, eventually reducing it to zero, which leads to $m = 0.013$, as shown in Fig. 7. Such a small magnetization can be explained by the finite-size effect in the absence of ordering. Disappearance of the magnetization is accompanied by the decrease of the energy in Fig. 8 down to $(E - E_0)/J = -0.19246$. The fraction of singularities in the final state is $f_s = 1.84 \times 10^{-5}$. One can see that for the 3d Heisenberg model the energy increase due to the creation of singularities as spins align with the RF is smaller than the energy gain due to the aligning. Although relaxation from the collinear initial state stops at a finite m because of the singularities (see the middle panel of Fig. 2), a more sophisticated process of the magnetic field sweep with decreasing amplitude helps the system to attain lower energy by disordering completely. The spin-spin correlation function in the final disordered state shown in Fig. 9 is close to the LIM exponential form. Slightly lower correlations in the numerical result can be explained by hedgehogs.

6 Magnetization of the F-state vs random-field strength

Another way to obtain the F-states is, starting from a collinear state, to increase the strength of the random field H_R from zero in small steps. [3] This procedure leads to the F-states with a smaller magnetization than that obtained directly by the relaxation from a collinear state. Results for magnetization and energy for the 3d xy model at $H_R/J = 1.5$ are $m = 0.467$ and $(E - E_0)/J = -0.14425$. New computation for $H_R/J = 1.5$ and $L = 512$, Figs. 10, 11, and 12, yields $m = 0.486$ and $(E - E_0)/J = -0.14415$ for the xy model and $m = 0.146$ and $(E - E_0)/J = -0.19226$ for the Heisenberg model. Comparison of these results with those above shows that the energy landscape

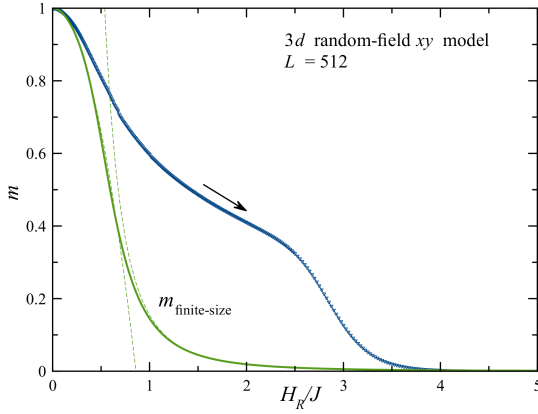


Fig. 10. Magnetization vs the RF strength H_R for the 3d xy model, $L = 512$. Green line is the finite-size magnetization expected in the absence of ordering. Dashed green lines are given by Eqs. (31) and (33).

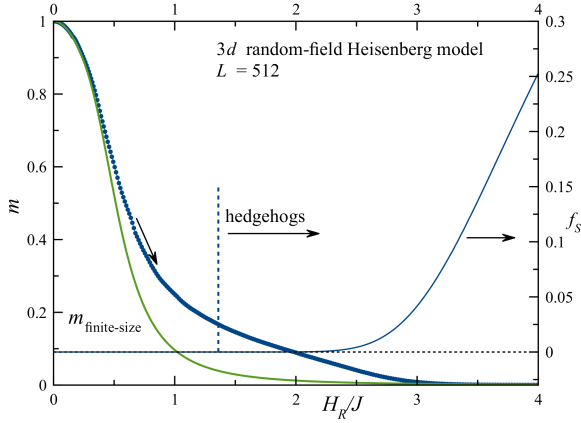


Fig. 11. Magnetization vs the RF strength H_R for the Heisenberg model, $L = 512$. Green line is the finite-size magnetization expected in the absence of ordering.

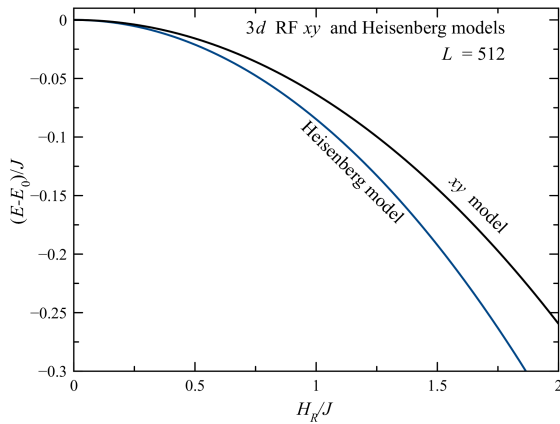


Fig. 12. Energy vs the RF strength H_R for the xy and Heisenberg models, $L = 512$.

of the RF model is very flat and states with markedly different magnetizations have very close energies.

The computed magnetization should be compared with the finite-size magnetization expected in the absence of ordering in the intermediate range of H_R . The latter can be obtained analytically in the regions $R_f \gg L$ and $R_f \ll L$, where the magnetic correlation range R_f is given by Eq. (16) and $h \equiv H_R$. For small H_R one has $R_f \gg L$ and the short-range order extends over the whole system, making the magnetization $m \cong 1$. Deviations from this short-ordered state can be found perturbatively. For the cube of size L with periodic boundary conditions the result has the form

$$m \cong 1 - A \frac{L}{R_f} \cong \left(1 + A \frac{L}{R_f}\right)^{-1}, \quad (31)$$

where

$$A = \frac{1}{4\pi^3} \sum_{n_x, y, z = -\infty}^{\infty} \frac{1}{(n_x^2 + n_y^2 + n_z^2)^2} \simeq 0.1333 \simeq \frac{4}{30}. \quad (32)$$

In the case $R_f \ll L$, assuming the exponential spin correlation function of Eq. (23) (that has been derived analytically for $n = \infty$ in Section 2 and confirmed numerically [1] for 3d models with $n > d + 1$) one obtains[3]

$$m \cong \sqrt{8\pi} \left(\frac{R_f}{L}\right)^{3/2} \quad (33)$$

(the so-called “fluctuational” or finite-size magnetization). One can build a good interpolation formula in the whole range of R_f that reads

$$m = \frac{1}{\sqrt{1/m_1^2 + 1/m_2^2}}, \quad (34)$$

m_1 and m_2 being the two limiting expressions above, Eqs. (31) and (33).

One can see that for the 3d xy model in Fig. 10 the computed magnetization is substantially larger than the finite-size magnetization given by Eq. (34) in the intermediate range of H_R . For small H_R the system is short-range-ordered, $m \cong 1$. For large H_R spins are forced to align with the random field and the system is completely disordered. The quasi-plateau of $m(H_R)$ followed by the shoulder at $H_R/J \simeq 2.5$ is due to the effect of vortex loops. As further decrease of m requires creating vortex loops that cost energy, the system remains ordered. [1] This holds until the RF overpowers the exchange.

An interesting fact is the reversibility of the $m(H_R)$ curve (in a limited range of H_R) that contrasts the hysteresis of $m(H)$ characterized by Barkhausen jumps. As H_R increases the spins turn more and more in the direction of the random field without overcoming any barriers. This suggests that the obtained state is generically related to the collinear ground state of a pure ferromagnet. Reaching $H_R/J \simeq 2$ causes creation of vortex loops, at which point the reversibility of the $m(H_R)$ curve breaks down. Thus

the F-states obtained by the adiabatic increasing of H_R are likely to have the lowest energy among all the F-states.

The results for the 3d Heisenberg model ($n = 3$) shown in Fig. 11 reveal a much smaller magnetization of the adiabatic F-state than for the xy model ($n = 2$). Even for the system size as large as $L = 512$, the computed magnetization is not much greater than the finite-size magnetization. This is because the F-state in the Heisenberg model is topologically protected by hedgehogs. The latter have much smaller energy than vortex loops of the xy model. Still, the nearly constant slope of $m(H_R)$ in the region $1 \lesssim H_R/J \lesssim 3$ indicates the existence of the ordered state that is slowly destroyed by emerging singularities – hedgehogs. The fraction of hedgehogs f_S is shown on the right axis of Fig. 11.

7 Numerical implementation of the Imry-Ma argument

Imry and Ma (IM) argument [6] assumes that in RF models the spins are directed along the random field averaged over correlated volumes of linear size R , found self-consistently by minimizing the energy due to the random field and exchange. The energy per spin is estimated as

$$E - E_0 \sim -sh \left(\frac{a}{R} \right)^{d/2} + s^2 J \left(\frac{a}{R} \right)^2, \quad (35)$$

where E_0 is the energy per spin of a collinear state. The first term in this formula is the statistical average of the RF energy in the IM domain of size R while the second term is the exchange energy from smooth rotation of the magnetization between adjacent domains. Minimization of the energy with respect to R yields $R = R_f$, where

$$R_f \sim a \left(\frac{sJ}{h} \right)^{2/(4-d)}. \quad (36)$$

For $d = 3$, up to the dependence on n , it coincides with Eq. (16). The resulting energy of the IM state is

$$E - E_0 \sim -s^2 J \left(\frac{h}{sJ} \right)^{4/(4-d)}, \quad (37)$$

that yields $E - E_0 \sim -h^4/J^3$ in a 3d field model.

It can be shown[1] that the IM state of the 3d xy model inevitably contains vortex loops that cost energy. The resulting estimation for the exchange becomes[3]

$$E_{\text{ex-V}} \sim s^2 J \left(\frac{a}{R} \right)^2 \ln \left(\frac{R}{a} \right) \quad (38)$$

that replaces the second term in Eq. (35). Minimization of the total energy then yields $R = R_f$, where

$$R_f \sim a \left(\frac{Js}{h} \right)^2 \ln^2 \left(\frac{Js}{h} \right) \quad (39)$$

c.f. Eq. (36). The resulting energy of the IM state then becomes[3]

$$E - E_0 \sim \frac{h^4}{s^2 J^3} \frac{1}{\ln^3(sJ/h)}. \quad (40)$$

In the case of a weak RF the large logarithm in the denominator significantly decreases the energy gain due to the adjustment of spins to the averaged RF. It should be stressed that the formula above is only an estimation and there can be unaccounted large numerical factors, in particular, in the argument of the logarithm.

In the lattice model the main contribution to the adjustment energy arises at the atomic scale and is given by $E - E_0 \sim -h^2/J$ in all dimensions. The IM energy represents small correction to that energy due to the large-scale rotation of the magnetization on a large distance R_f . Finite value of R_f for any $d < 4$ supports the IM picture of a disordered state. However, it does not prove rigorously that the ground state of the system has $m = 0$. To prove that one has to compare the energy of the $m = 0$ state, that may contain topological defects, with the energy of defect-free F-states with $m \neq 0$.

Mathematical implementation of the averaged RF is

$$\bar{\mathbf{h}}_i = \sum_j K_{ij} \mathbf{h}_j, \quad (41)$$

or, within the continuous approximation,

$$\bar{\mathbf{h}}(\mathbf{r}) = \int d^d \mathbf{r}' K(\mathbf{r}') \mathbf{h}(\mathbf{r}' + \mathbf{r}), \quad (42)$$

where K an averaging kernel. Spins follow the direction of $\bar{\mathbf{h}}$ and have to be normalized,

$$\mathbf{s}(\mathbf{r}) = s \frac{\bar{\mathbf{h}}(\mathbf{r})}{|\bar{\mathbf{h}}(\mathbf{r})|}. \quad (43)$$

The choice of the averaging kernel introduces uncertainty into the IM construction. Possible choices for $K(r)$ are rigid sphere, rigid cube, Gaussian, exponential, etc.

For the δ -correlated random field, Eqs. (3) or (12), the correlator of the averaged RF is given by

$$\langle \bar{h}_\alpha(\mathbf{r}) \bar{h}_\beta(\mathbf{r}') \rangle = \frac{h^2}{n} \delta_{\alpha\beta} \Gamma(|\mathbf{r} - \mathbf{r}'|), \quad (44)$$

where

$$\Gamma(r) = \frac{1}{a^d} \int d^d \mathbf{r}' K(\mathbf{r}') K(|\mathbf{r} - \mathbf{r}'|). \quad (45)$$

Thus the averaged RF is a correlated RF. We will require $\Gamma(0) = 1$ that yields the condition

$$1 = \frac{1}{a^d} \int d^d \mathbf{r} K^2(r). \quad (46)$$

Choosing different $K(r)$, one can obtain different $\Gamma(r)$. Considering, instead of Eq. (43), spin vectors

$$\mathbf{s}(\mathbf{r}) = s \frac{\bar{\mathbf{h}}(\mathbf{r})}{h} \quad (47)$$

that are normalized on average amounts to the mean spherical model (see Sec. 2). The correlation function of these spins is exactly $\Gamma(r)$. The actual spins, however, have to be normalized at each site by Eq. (43). The denominator in Eq. (43) introduces singularities in the spin field where $|\bar{\mathbf{h}}(\mathbf{r})| = 0$. This happens forcibly, if the number of spin components n is small enough, $n \leq d$, that includes practical cases.[1] For $n > d$ there is no topological reason for $|\bar{\mathbf{h}}(\mathbf{r})| = 0$, and one can expect that the difference between the spin fields defined by Eqs. (43) and (47) is small.

Let us consider particular averaging kernels. The rigid-cube kernel satisfying Eq. (46) is given by

$$K(\mathbf{r}) = \begin{cases} [a/(2R)]^{d/2}, & |x|, |y|, |z| \leq R \\ 0 & |x|, |y|, |z| > R. \end{cases} \quad (48)$$

The correlation function Γ is defined by the overlap area of two shifted cubes that leads to the small-distance behavior

$$1 - \Gamma(r) \sim r/R. \quad (49)$$

Disappearance of the overlap leads to the vanishing of Γ at finite distances, an undesirable property.

The Gaussian averaging kernel in 3d is given by

$$K(r) = \left(\frac{2}{\sqrt{\pi}} \frac{a}{R} \right)^{3/2} e^{-2(r/R)^2}. \quad (50)$$

The corresponding RF correlation function is

$$\Gamma(r) = e^{-(r/R)^2}. \quad (51)$$

One can see that this result disagrees with the spin-spin correlation function that follows from the Green-function method, as well as with Eq. (23) for the mean spherical model.

The exponential averaging kernel in 3d is given by

$$K(r) = \frac{1}{\sqrt{\pi}} \left(\frac{a}{R} \right)^{3/2} e^{-r/R}. \quad (52)$$

The corresponding RF correlation function is non-exponential and goes quadratically at small distances,

$$\Gamma(r) \cong 1 - \frac{1}{6} \left(\frac{r}{R} \right)^2, \quad r \ll R \quad (53)$$

again contradicting and has the long-distance behavior

$$\Gamma(r) \cong \frac{1}{3} \left(\frac{r}{R} \right)^2 e^{-r/R}, \quad R \ll r, \quad (54)$$

again, contradicting Eq. (23).

On the contrary, Yukawa averaging kernel in 3d

$$K(r) = \frac{a^{3/2}}{\sqrt{2\pi} R} \frac{1}{r} e^{-r/R} \quad (55)$$

that has the same singularity as the Green function of the mean-spherical model ($n = \infty$), leads to the desired exponential correlation function of the correlated RF

$$\Gamma(r) \cong e^{-r/R} \quad (56)$$

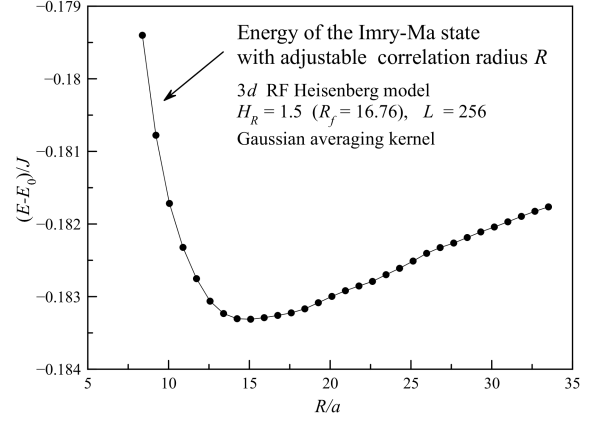


Fig. 13. Energy of the constructed IM state in the 3d Heisenberg model vs the averaging range R . Gaussian averaging kernel is used and the short-range energy of Eq. (30) is added.

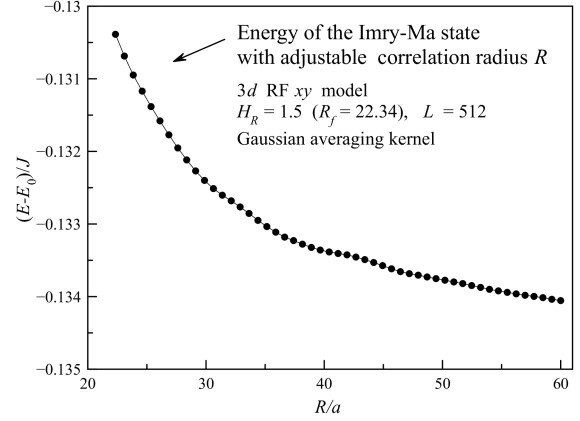


Fig. 14. Energy of the constructed IM state in the 3d xy model vs the averaging range R . Gaussian averaging kernel is used and the short-range energy of Eq. (30) is added.

and thus of the spin-spin correlation function for spins normalized on average. This is not surprising because for the Yukawa kernel Eqs. (42) and (47) are equivalent to Eq. (21) that results in Eq. (23).

Let us consider the energies of the constructed IM states, using the simplified form of the spin field given by Eq. (47). Then $\Gamma(r)$ above is the spin-spin correlation function. The exchange energy is defined by the nearest-neighbor correlation function, thus

$$E_{\text{ex}} - E_0 = s^2 dJ [1 - \Gamma(a)], \quad (57)$$

where $E_0 = dJ$ is the ground-state energy of a pure magnet. This method of computing the exchange energy used in Ref. [3] ignores lattice-discreteness effects at small distances. However, it can be shown that the error is very small. One can see that $E_{\text{ex}} - E_0 \propto 1/R$ for the rigid cut-off and Yukawa averaging kernels and $E_{\text{ex}} - E_0 \propto 1/R^2$ for the Gaussian and exponential averaging kernels. As the second case is in accord with the IM argument, this type of kernels will be called regular.

The random-field energy per spin is given by $E_{RF} = -\langle \mathbf{s}_i \cdot \mathbf{h}_i \rangle$. Using Eq. (47), one obtains

$$E_{RF} = -\frac{s}{h} \langle \bar{\mathbf{h}}_i \cdot \mathbf{h}_i \rangle = -\frac{s}{h} \left\langle \sum_j K_{ij} \mathbf{h}_j \cdot \mathbf{h}_i \right\rangle \\ = -shK_{ii} = -shK(0). \quad (58)$$

For regular kernels as well as for the rigid cut-off kernel in 3d, using Eqs. (50) and (52), one obtains $E_{RF} \propto -1/R^{3/2}$, as in the IM argument. In fact, there is an agreement of both exchange and random-field energies with their IM forms for any dimension d , if regular averaging kernels are used. Minimizing the total energy with respect to R , one obtains the value of R_f above and the minimal energy $E - E_0 \propto -h^4/J^3$ in 3d, according to Eq. (37). Thus, regular averaging kernels fully reproduce the original IM argument [6] and provide its implementation with the results differing only by a numerical factor.

However, using regular kernels one misses the main contribution to the energy due to the adjustment of spins at the atomic scale, $E - E_0 \propto -h^2/J$. [3] Another drawback of these kernels is the wrong spin-spin correlation function in 3d.

For the Yukawa averaging kernel, Eq. (58) is singular within the continuous approximation. However, the lattice Green function with coinciding indices is finite. The regularization can be done by the replacement $r \rightarrow a$ in the denominator of Eq. (55). The corresponding modification yields

$$K_{ii} = \eta \sqrt{\frac{a}{2\pi R}}, \quad (59)$$

where η is a constant. The total energy for the Yukawa averaging kernel following from Eqs. (56), (57), (58) and the formula above in 3d is given by

$$E - E_0 = 3s^2 J \frac{a}{R} - sh\eta \sqrt{\frac{a}{2\pi R}}. \quad (60)$$

Minimizing this energy over R yields

$$\frac{R_f}{a} = 8\pi \left(\frac{3J}{\eta h} \right)^2 \quad (61)$$

and

$$E_{\text{ex}} - E_0 = \frac{\eta^2 h^2}{24\pi J}, \quad E_{RF} = -2(E_{\text{ex}} - E_0). \quad (62)$$

Choosing $\eta^2 = 9(1 - 1/n)$, one recovers R_f of Eq. (36) and the total adjustment energy of Eq. (30). Summarizing, using the Yukawa averaging kernel in the IM construction provides correct forms of the spin correlation function, including the magnetic correlation length R_f , as well as the leading contribution to the energy h^2/J . In the limit $n \rightarrow \infty$ the results above become exact and coincide with those of the mean spherical model.

The approach proposed above allows to numerically minimize the energy of the system on the magnetic correlation range, i.e., the averaging range R . As the spirit

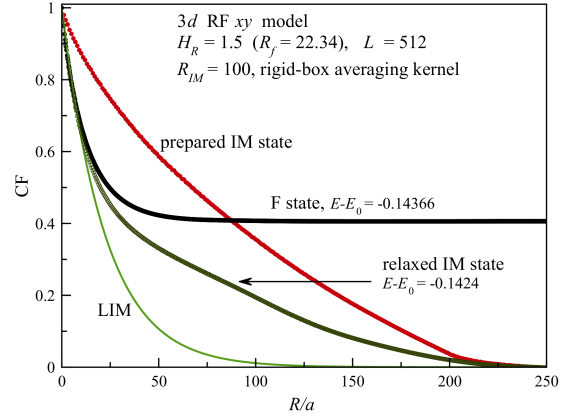


Fig. 15. Spin-spin correlation function of the constructed IM state with the rigid-cube cut-off and of the corresponding relaxed state. The spin-spin correlation function of the F-state and the theoretical LIM curve are shown for comparison.

of the original Imry-Ma argument requires a non-singular averaging kernel, we will use the Gaussian kernel that reproduces both terms of the basic equation (35). For the 3d Heisenberg model in Fig. 13, there is clearly the energy minimum at $R/a \simeq 15$ that is close to $R_f/a = 16.76$. One can see that singularities of the spin field, hedgehogs, do not disturb much the IM argument. On the contrary, for the 3d xy model, we were unable to find the energy minimum for $H_R/J = 1.5$ up to the rather large values of R , as can be seen in Fig. 14. This striking effect can be attributed to vortex loops that inevitably arise in the completely disordered 3d xy model[1] and increase the exchange energy by a large factor $\ln(R/a)$, Eq. (38), making it decrease slower with R . On the top of it, one has to suggest a large numerical factor in the argument of the logarithm that is absent in the simple estimation above. The bottom line is that numerical implementation of the Imry-Ma construction with "traditional" non-singular averaging kernels does not work for the 3d xy model. This is not a surprise given that non-singular kernels result in a wrong spin correlation function.

As non-singular averaging kernels do not describe the short-range adjustment energy h^2/J , Imry-Ma states obtained with the help of them possess a too high energy. Thus they have to be relaxed numerically to reach the actual energy corresponding to a local energy minimum. Below we will show the results for the rigid-cut-off, Gaussian, and Yukawa kernels.

The spin-spin correlation function for the rigid-cut-off state with $R = R_{IM} = 100$ is shown in Fig. 15. It has a characteristic shape with a nearly-constant slope ending at the distance $2R$. This shape is very different from the IM exponential correlation function that follows from the Green function method. Starting from this constructed IM state, numerical minimization of the energy with $H_R/J = 1.5$ was performed. The resulting spin-spin correlation function also shown in the figure coincides with the IM curve and with the correlation function of the

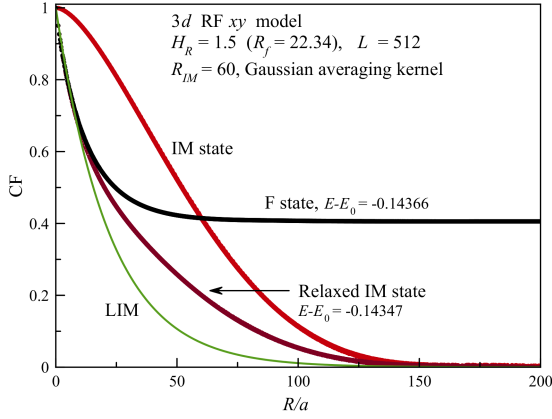


Fig. 16. Spin-spin correlation function of the constructed IM state with the Gaussian averaging kernel and of the corresponding relaxed state. The spin-spin correlation function of the F-state and the theoretical LIM curve are shown for comparison.

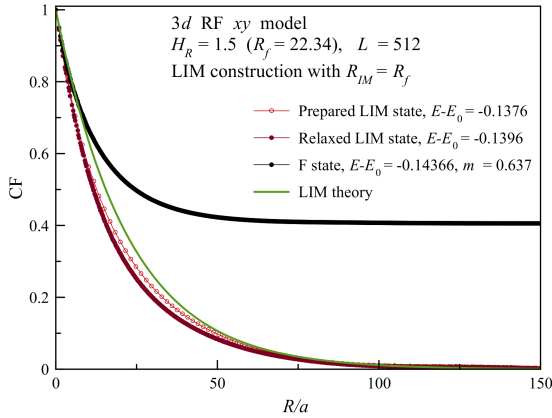


Fig. 17. Spin-spin correlation function of the constructed IM state with the Yukawa averaging kernel and of the corresponding relaxed state. The spin-spin correlation function of the F-state and the exponential LIM curve are shown for comparison.

F-state at the distances $r \lesssim R_f$, where $R_f/a = 22.34$. At larger distances this correlation function is decreasing slowly, similarly to the constructed IM correlation function, and it turns to zero at the same distance. This result implies that at distances $r \lesssim R_f$ the system relaxes to minimize its energy, whereas at larger distances the system is pinned by the RF and its state depends on the initial state.

Similar results were obtained with the Gaussian averaging kernel, see Fig. 16. Energies of the relaxed IM states in both figures above are slightly greater than the energy of the F-state. This means that long-distance correlations can be changed at a very small energy cost, similarly to creating a domain wall in a big system.

The results for the IM construction with the Yukawa averaging kernel for the 3d xy model are shown in Fig. 17. Here also $H_R/J = 1.5$ was used, and the constructed

state was created with the actual spin correlation range $R_f/a = 22.34$. Since spins are normalized by Eq. (43) this creates singularities, the spin-spin correlation function goes slightly below the LIM curve, as can be seen in Fig. 17. Subsequent relaxation makes the correlation function go slightly lower than the IM curve. The energies of both, the constructed IM state and the corresponding relaxed state, are close to that of the F-state but still higher. This is because the constructed IM state and the relaxed state possess vortex loops that cost energy.

One can conclude that the singular Yukawa averaging kernel provides a much better approach to the structure of the disordered magnetic states than non-singular averaging kernels in the spirit of the original Imry-Ma argument.

Energies of the relaxed states obtained from the constructed IM states with a large correlation range, see Figs. 15 and 16, are slightly above the energy of the F-state. These states have a two-scale structure defined by R_f of Eq. (36) and the initial large correlation range. As the energy of pinned state at the scale $R \gtrsim R_f$ in the computations above is not minimized, one can imagine that one could find a state with the energy that is lower than that of the F-state. This presumably can be done by slowly rotating the F-state on a characteristic scale $R' \gg R$. At first glance it appears obvious that this would win an additional Zeeman energy $-\mathbf{m} \cdot \langle \mathbf{h} \rangle$, where $\langle \mathbf{h} \rangle$ is the random field averaged on the scale R' . The obvious candidate for R' in a 3d xy model is the IM length with account of one vortex loop per IM domain, Eq. (39). Such a ground state would have zero magnetization. It would have two scales: R_f characterizing the partial disordering of the magnetization inside F-state domains of size $R' \gg R$ that are oriented randomly with respect to each other, with a smooth rotation of \mathbf{m} between the domains. Notice that in the absence of a proof, one also cannot exclude the possibility that in this two-scale ground state the magnetization of the F-state domains rotates randomly with a power-law decay of correlations at large distances as predicted by the Bragg glass theory. It should be noted that we do not have an analytical theory of this two-scale state. Also it is very difficult to obtain numerically because of the energy barriers and a very small energy gain.

8 Microscopic structure of the F-state

For arbitrary number of spin components n the correlation range R_f of the RF system perfectly agrees with the value calculated by the Green-function method, that is itself in a qualitative agreement with the Imry-Ma argument. For any n the spin-spin correlation function decreases as $C(r) \cong 1 - r/R_f$ at distances $r \lesssim R_f$. At $n > d + 1$ correlations decay exponentially regardless of the initial condition for the spins. [1] However, for $n \leq d$ at $r > R_f$ the correlation function of the state obtained by the relaxation from the fully ordered state has a plateau corresponding to a non-zero magnetization. The spin field in the F-state does not have singularities that would arise in the case of $n \leq d$ in the hypothetical Imry-Ma state in which spins

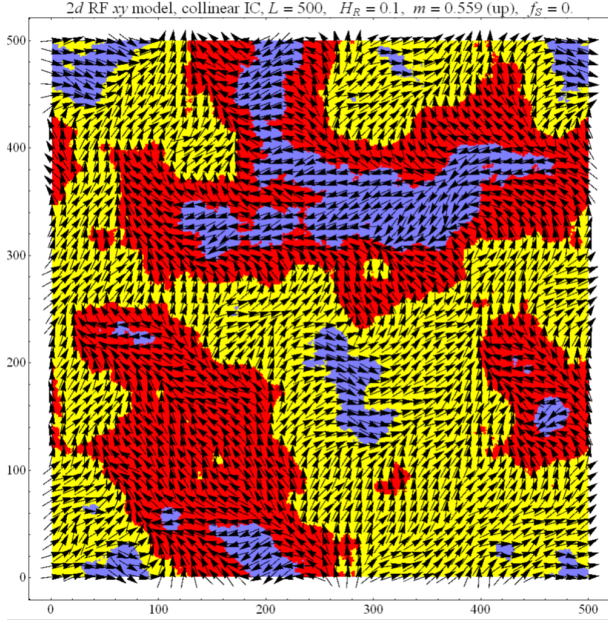


Fig. 18. Imry-Ma domains in the F-state of the $2d$ xy model at zero applied field. Only a fraction of spins are shown.

follow the RF averaged inside the IM domains of linear size R_f .

It is interesting to look at the difference between the F-state and the IM state by visualizing the domains. For this purpose, color labeling of the F-states in the $2d$ xy model obtained, as usual, by relaxation from a collinear state in zero applied field, has been done as shown in Fig. 18. With the sample's magnetization pointing up (positive y direction), regions with spins turned to the right are coded yellow and spins turned to the left are coded red. Spins directed down are labeled blue overriding yellow and red. The results can be understood as follows. Under the influence of the random field spins are rotating clockwise and counterclockwise from the initial direction up, becoming yellow and red. Rotating more into the down region, they become blue. In this scenario, blue regions are entirely inside their parent yellow and red regions and spins are divided into rotated clockwise and counterclockwise. This spin state is topologically equivalent to the initial collinear state and can be transformed back to it without creating or annihilating topological structures.

Color-coded regions in Fig. 18 can be interpreted as IM domains. Boundaries between yellow and red correspond to $s_x = 0$, whereas the boundaries between yellow and blue or between red and blue correspond to $s_y = 0$. As was shown in Ref. [3] the IM construction inevitably leads to the formation of vortices or anti-vortices on purely mathematical grounds. This does not happen when spins rotate clockwise or counterclockwise to form the F-state. In that state the spins do not follow the averaged random field precisely and the system disorders only partially, keeping the memory of the initial collinear state. Complete disordering is blocked because singularities would increase the system's energy.

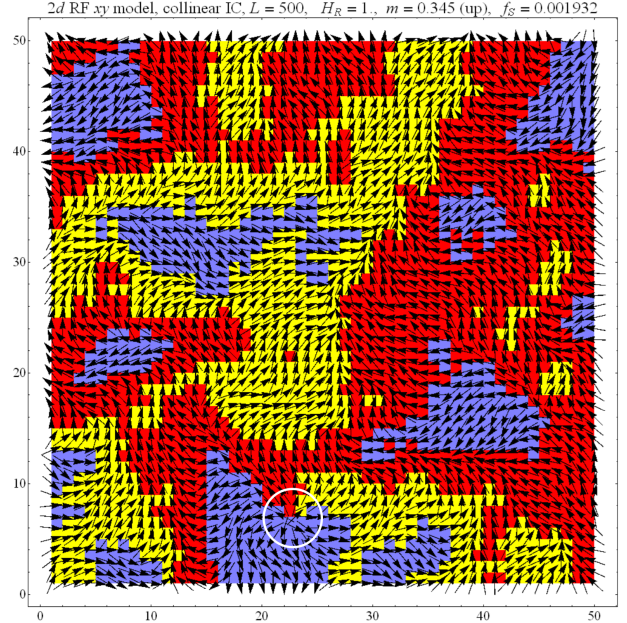


Fig. 19. Imry-Ma domains in the F-state of the $2d$ xy model at zero applied field, with a vortex in the lower part inside the white circle. Only a fraction of the lattice is shown.

If blue regions corresponding to the down spins rotated clockwise and counterclockwise merge, as can be seen near the bottom of Fig. 19, there would be an intersection of the yellow-red boundary with the red-blue and yellow-blue boundaries, that is, an intersection of the $s_x = 0$ and $s_y = 0$ lines. As the result, there is a white-encircled vortex in Fig. 19. Singularities, such as vortices, can be created by a strong enough random field out of a collinear state, as is the case in Fig. 19. One can see that the state shown in Fig. 19 has lost the memory of the initial collinear state and it cannot be returned to it without changing topology.

One can suggest the form of the IM argument that does not assume a complete disordering and is thus suitable for the description of F-states. [3] It takes into account the adjustment of spins to the random field at all length scales. Groups of spins of linear size R rotate by an adjustment angle ϕ (considered as small to begin with) under the influence of the components of the averaged random field perpendicular to the initial direction. The corresponding energy per spin is given by

$$E - E_0 \sim -sh \left(\frac{a}{R} \right)^{d/2} \phi + s^2 J \left(\frac{a}{R} \right)^2 \phi^2. \quad (63)$$

Minimizing this expression with respect to ϕ , one obtains

$$\phi \sim \left(\frac{R}{R_f} \right)^{(4-d)/2}, \quad (64)$$

where R_f is given by Eq. (36). The angular deviation increases with the distance and becomes large at $R \sim R_f$. The energy per spin corresponding to spin adjustment at the distance R can be obtained by substituting Eq. (64)

into Eq. (63). The result has the form

$$E - E_0 \sim -\frac{h^2}{J} \left(\frac{a}{R}\right)^{d-2}. \quad (65)$$

One can see that the highest energy gain is provided by spin adjustments at the atomic scale, $R \sim a$. In this case one obtains

$$E - E_0 \sim -h^2/J. \quad (66)$$

Substituting R_f of Eq. (36) into Eq. (65), one recovers the IM energy of Eq. (37). One can see that the IM energy in the F-state is of the same order of magnitude as the regular IM energy. Because of the incomplete adjustment of spins to the random field in the F-state, one can expect that its IM energy contains a smaller numerical factor than Eq. (37). Nevertheless, this energy should be lower than Eq. (40) because of the logarithmic factor in the latter.

9 Memory of the initial condition: Rotational elasticity of the F-state

The magnetization in the F-state can be pointed in any direction because of the macroscopic isotropy of the problem. This direction practically coincides with the magnetization direction in the initial collinear state. Macroscopic isotropy does not mean, however, that the magnetization in the F-state can be rotated at no energy cost, as it would be in the isotropic ferromagnet in the absence of the RF. The difference is that the magnetization in the F-state is pinned by a partial adjustment to the random field. It has a memory of the initial collinear state. Rotation of the magnetization of the sample, even by a small angle, requires readjustment of the local magnetization that is inhibited by local energy barriers.

An illustration of this memory effect is the dependence of magnetization components on the magnetic field perpendicular to the initial magnetization shown in Fig. 20. The magnetization component in the direction of the field m_H increases from zero with a *finite slope* because of pinning, whereas the magnetization component along the initial magnetization m_m decreases to zero. After aligning with the field at larger fields, the magnetization increases. One can see Barkhausen jumps in the magnetization curves. For smaller or larger values of H_R the dependence m_H is less linear and it is difficult to scale the results neatly.

Another, more pure, numerical experiment on the rotation of the magnetization in the F-state can be performed as follows. An F-state is prepared by the relaxation from a collinear state. Then a constrained energy minimization is performed with the magnetization direction fixed at the angle θ with its original direction.[52] The value of θ is gradually increased from zero in both directions for the 3d xy model. The corresponding Lagrange multiplier is an adjustable magnetic field perpendicular to the instantaneous sample's magnetization. The results of this numerical experiment shown in Fig. 21 confirm strong pinning of the F-state. The magnetization does not rotate easily in the

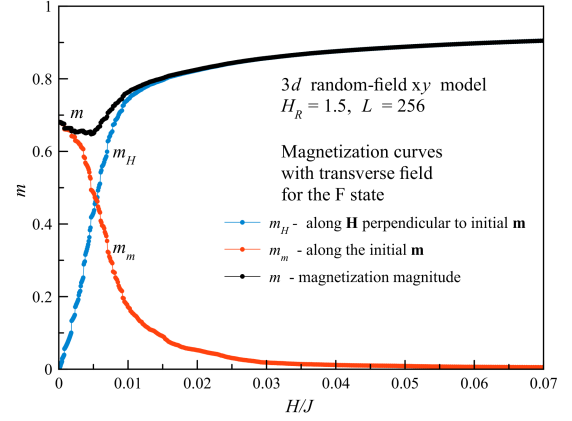


Fig. 20. Magnetization curves of the F-state in the 3d xy model in a transverse field.

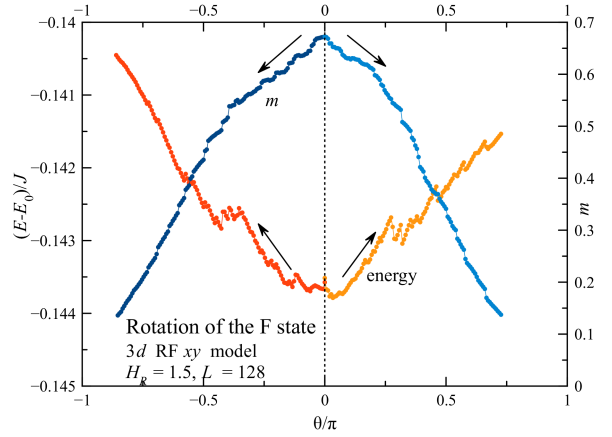


Fig. 21. Rotation of the F-state.

potential landscape created by the RF. Instead, it exhibits elasticity that can be interpreted as a memory of the initial state. While the energy increases for the rotation in any direction, the magnetization decreases to small values for which the method stops working.

10 Effects of temperature

10.1 Numerical method

At nonzero temperatures we replace the rotation spins towards the direction of the effective field by Monte Carlo updates,[43]. Sequentially at each lattice site, spins are rotated into a random direction within a cone around the initial spin direction. The width of the cone increases with the temperature in such a way that approximately half of new spin directions are accepted. According to the basic Monte Carlo routine, the new orientation is accepted if the new energy is lower than the old one. In the opposite case the new orientation is accepted with the probability $\exp[(E_{\text{old}} - E_{\text{new}})/T]$. The energy change due to rotation

of a single spin is a local quantity in our model, thus the method is parallelizable and fast.

We combine Monte Carlo spin updates with the energy-conserving over-relaxation (see Sec. 3), again with probabilities α and $1 - \alpha$, respectively. At high temperatures $\alpha = 1$ provides the fastest relaxation to the equilibrium. However, at low temperatures the method with small α becomes more efficient. This is similar to the behavior of the relaxation routine used at $T = 0$. For large α , the system quickly falls into the nearest shallow energy minimum (actually a multi-dimensional energy valley) and begins a long trip along it. For small α , the system first finds the maximum-entropy state that corresponds to a broad and deep energy basin and then descends into the corresponding minimum.

As the stopping criterion for equilibration, we require that the drift of the energy value averaged over the interval n_{avr} of Monte Carlo updates within this interval becomes smaller than the statistical scatter of the energy. The greater n_{avr} , the stricter is the equilibration criterion. In the data below we used $n_{\text{avr}} = 30$.

Examples of Monte Carlo energy relaxation out of the collinear and random initial states for $\alpha = 1$ and 0.1 are shown in Fig. 22. One can see that for the temperature as low as $T/J = 1$ for $\alpha = 0.1$ the system relaxes to nearly the same energies from both collinear and random initial states. On the other hand, for $\alpha = 1$ relaxation out of the random state becomes too slow. At this temperature, states reached from random and collinear initial conditions are different. Collinear initial condition results in F states while random initial condition results in the magnetically disordered vortex-glass state. The energy difference between these states is not seen in this scale. At higher temperatures, the system relaxes into the same magnetically disordered state out of both random and collinear initial conditions. This case is non-problematic and the method with $\alpha = 1$ is the fastest.

After the stationary values of the energy and magnetization have been reached, we typically perform 200 Monte Carlo updates to measure the physical quantities. Due to the large system size, thermodynamic fluctuations, as well as the difference between various realizations of the random field, are small. The statistical scatter seen in the figures is also small and it is not masking the qualitative features.

10.2 Numerical results

In this Section we consider effects of finite temperature with the help of the Monte Carlo Metropolis algorithm combined with over-relaxation. The relevant questions are whether the system orders spontaneously on cooling and whether finite temperature leads to the full disordering of the F-state by helping the system to overcome energy barriers.

The answer to the first question is negative. On cooling, the $3d$ xy system freezes into the vortex-glass (VG) state with a small magnetization being a finite-size effect. The energy of the VG state is higher than that of the

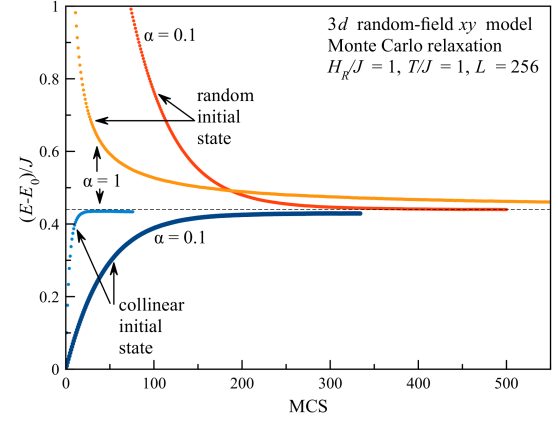


Fig. 22. Energy relaxation in the Monte Carlo routine.

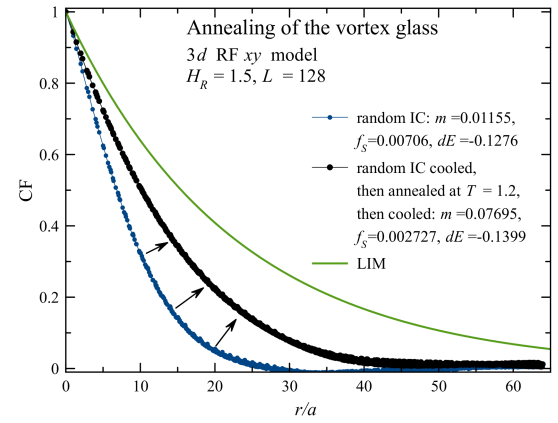


Fig. 23. Annealing of the vortex-glass state.

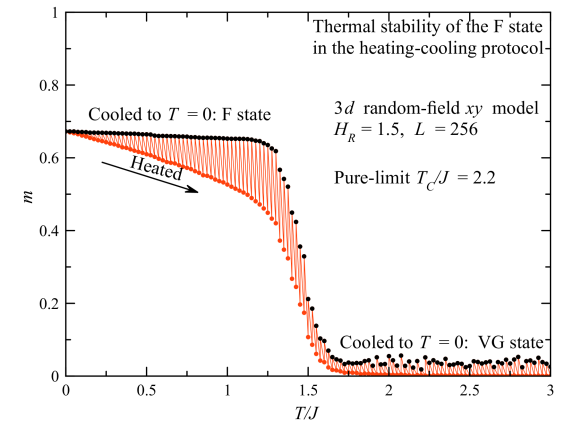


Fig. 24. Heating-cooling protocol for the $3d$ xy model. The temperature is increased in steps and each time dropped to zero.

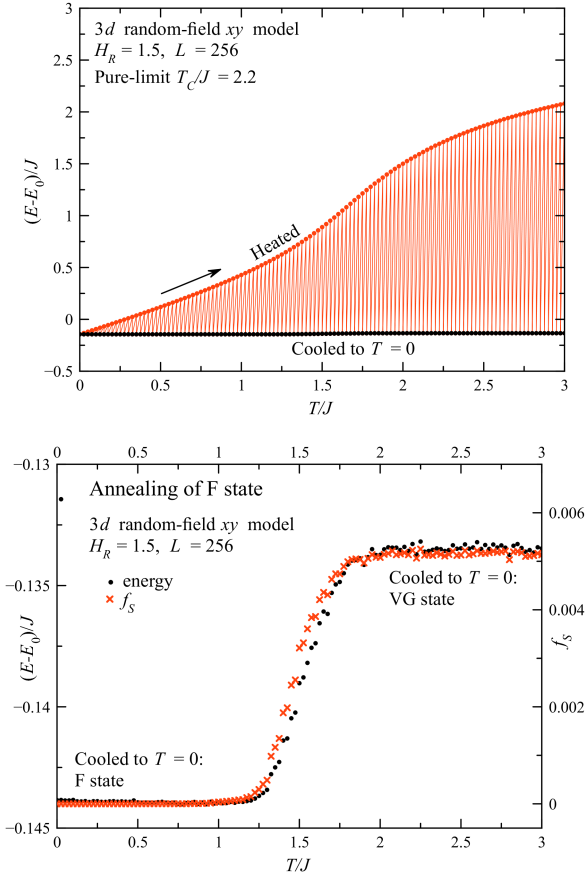


Fig. 25. Energy in the heating-cooling protocol for the 3d xy model. Lower panel: Magnification of the $T = 0$ results.

F-state because of pinned vortex loops. [3] Numerical investigation shows that the VG state is not unique and depends on preparation. Relaxation from a random state at $T = 0$, even using the algorithm with a slow energy loss, $\alpha \ll 1$, leads to the VG states with more vortices and higher energies. Stepwise lowering temperature leads to the VG states with less vortices and lower energies. As singularities in the spin field are breaking spin-spin correlations, the correlation functions of states with more singularities decay faster. To illustrate this point, annealing of the VG state of the 3d xy model with $H_R = 1.5$ obtained by relaxation from a random state at $T = 0$ has been done. After initial relaxation at $T = 0$, the temperature was raised to $T/J = 1.2$ and the system was equilibrated. After that the temperature was again dropped to zero. The obtained annealed state has lower vorticity and lower energy, while its correlation range is longer, as can be seen in Fig. 23. Annealing helps to depin and kill some vortex loops, while stronger pinned loops survive. Heating the system to even higher temperature would depin more vortex loops. However, this would create new ones. As a result, the annealing cannot eliminate vortex loops completely and it cannot bring the system from the VG state to the vortex-free state.

Next, we investigate thermal stability of the F-state by a heating protocol that consists of stepwise heating of the initial F-state to higher temperatures, each time allowing the system to relax at $T = 0$. The temperature sequence has the form $(0, T_1, 0, T_2, 0, T_3, \dots)$ with $T_1 < T_2 < T_3 \dots$. States with non-zero temperature are obtained with the Metropolis Monte Carlo routine, while zero-temperature states are obtained by the method of Ref. [3] that includes direct rotations of spins toward the effective field and over-relaxation. Since in this method the fraction of over-relaxation steps is dominant and the system is relaxing slowly, we do not call this sequence “annealing-quenching”. The magnetization results of this numerical experiment for the 3d xy model are shown in Fig. 24. For the temperatures below $1.2J$, the system returns to the F-states. Heating to higher temperatures creates vortex loops that get pinned and do not collapse upon dropping T to zero. Thus the F-state gets destroyed by heating to higher temperatures, the resulting state being the VG state.

The energy in the heating-cooling protocol is shown in Fig. 25. In the upper panel, the non-zero-temperature branch has the largest slope (the maximum of the magnetic heat capacity) around $T/J = 1.6$ for $H_R/J = 1.5$ used here. In the absence of the RF there is a ferromagnetic phase transition at $T/J = 2.2$. The $T = 0$ branch in the upper panel looks like a straight line. However, its magnification in the lower panel shows a fine structure with the crossover from the F-state to the higher-energy VG state above $T/J = 1.2$. The energy of the VG state perfectly correlates with the fraction of singularities. [3]

We also have performed the heating-cooling experiment for a 3d Heisenberg model. The results shown in Fig. 26 are similar to those for the xy model above. Since hedgehogs in the Heisenberg model carry much less energy than the vortex loops in the xy model, the energy of the hedgehog-glass (HG) is only slightly above that of the F-state.

11 Discussion and Conclusions

We have presented a comparative study of glassy states of three-dimensional xy and Heisenberg random-field models. The xy spin model is conceptually similar to the model of a pinned flux lattice, even though the symmetry of the two models is slightly different. [43] The Heisenberg RF model has practical implementation in antiferromagnets with quenched disorder. [15] Some of the properties of the two models may be also relevant to properties of amorphous and sintered magnets, although there are very significant differences between the effects of the random field and random anisotropy.

Earlier we have found that the properties of the random-field model are controlled by topology. [1] For the n -component spin in d dimensions the reversible behavior with exponential decay of correlations occurs at $n > d + 1$ when topological defects are absent. At $n \leq d$ the random-field system possesses pinned topological defects and exhibits glassy behavior. The focus of this paper has been on the

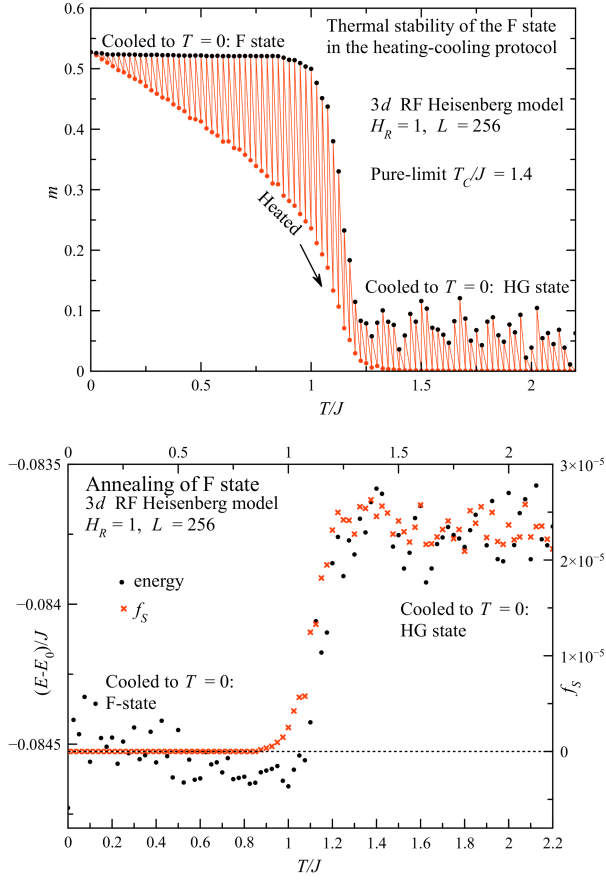


Fig. 26. Heating-cooling protocol for the 3d Heisenberg model. Lower panel: Energy and singularity fraction at $T = 0$.

properties of the F-state obtained by relaxation from the initially ordered state. One of our main findings is a profound difference between the F-states of the xy model and the Heisenberg model. While the latter can be transformed into a lower energy state with $m = 0$ by applying an appropriate hysteresis cycle, the xy F-state appears robust against attempts to lower its energy and decrease the magnetization at the same time. This can be traced to the inevitable presence of topological defects in the $m = 0$ state at $n \leq d$. [3, 1] In the 3d Heisenberg model such defects are hedgehogs that have relatively low energy as compared to the vortex loops in the 3d xy model. It is the reluctance of the xy RF system to form high-energy vortex loops that makes the F-state robust with respect to disordering.

Our other interesting finding is that the F-state possesses memory of the initial state. There is an infinite number of F-states that differ from each other by the direction of the global magnetic moment determined by the initial ordered state that the F-state has evolved from. Unlike in a ferromagnet with the exchange interaction only, these states are separated by energy barriers due to the random field. Small rotation of the magnetization of the F-state reveals its elasticity: rotation generates forces that return \mathbf{m} to its original direction. This makes one wonder whether

the F-state has any relevance to the elastic glass discussed in the past. [31, 39]

We have also studied the effect of temperature on the F-state. Naively, one would expect that it can be easily annealed towards thermal equilibrium. Our results do not support this expectation. While heating helps to depin topological defects, it also creates the new ones. Annealing of the vortex glass state does result in the lower vorticity and lower energy but it cannot eliminate vortices completely. On the contrary, heating and cooling of the F-state generates vortex loops that have been completely absent at the beginning. This reduces the magnetization but also leads to the higher energy than the energy of the F-state not subjected to the heating-cooling procedure. The bottom line is that the RF system, when cooled down after exposure to elevated temperature, behaves as a glass. It stores the thermal energy in the form of pinned topological defects.

There is a deep analogy between this state and the state of a conventional bulk ferromagnet with defects. In the case of the conventional ferromagnet the magnetization and the internal dipolar field adjust self-consistently through equations of magnetostatics. In a similar manner, the magnetization of the RF system adjusts self-consistently to the average random field. When cooled in a zero field below the Curie temperature, a conventional ferromagnet ends up in a state with small domains and high energy dominated by pinned domain walls. Similarly, the RF magnet ends up with many pinned topological defects: vortex loops in the xy model and hedgehogs in the Heisenberg model. When relaxing from a magnetized state at a sufficiently low temperature, a conventional ferromagnet ends up in a state with a finite magnetization because domain walls cannot easily penetrate in the magnet due to pinning and, thus, cannot form the $m = 0$ ground state. In a similar manner, the RF magnet ends up in the F-state when it relaxes from the ordered initial state. There are significant differences though as well. The $m = 0$ ground state of a conventional ferromagnet is the minimum of magnetostatic energy that has not been considered in the context of the RF system studied by us and by other authors. It is not at all obvious whether the xy system in the F-state can lower its energy by accommodating a large vortex loop that would reduce the magnetization to zero. Although there may be little profit in discussing the ground state of the glassy system, some remarks are in order.

The Imry-Ma argument is clearly valid at the qualitative level as long as the $m = 0$ state does not require topological defects. [1] At $n \leq d$ the argument becomes less obvious as the IM domains cannot be formed without topological defects. On the first glance, it appears that topological defects only modify the IM argument but do not destroy it. Indeed, in a 3d xy model there would be roughly one vortex loop per IM domain of size R . The energy of the loop would be of order $2\pi J s^2 (R/a) \ln(R/a)$, that corresponds to the energy $2\pi J s^2 (a/R)^2 \ln(R/a)$ per spin. This modifies the exchange energy in Eq. (35) by a factor proportional to $\log(R)$ and leads to a greater but

still finite R_f in the disordered state. The energy lowering due to the formation of the IM state becomes strongly reduced when vortex loops are present, see Eq. (40). At the same time, the lowering of the energy in the vortex-free F-state, see Eq. (63) and below, remains of the same order as the regular IM lowering described by Eq. (37).

For the 3d Heisenberg model, the energy of a hedgehog in the domain of size R is $4\pi J s^2 (R/a)$, which modifies the exchange energy per spin and the resulting IM energy by a factor of order unity. This makes estimates of the energies of the disordered IM state with hedgehogs and the F-states without hedgehogs the same. Making hysteresis loops with decreasing amplitude converts the F-state into a disordered state of the lower energy. This indicates that the ground state of the 3d Heisenberg model may be disordered in spite of hedgehogs.

One should note that in the presence of topological defects the IM argument becomes less precise as it ignores misalignment of the spin field with the average random field due to defects, as well as the interaction between topological defects. There is also a scaling argument that makes the IM argument even less obvious. Indeed, the IM argument relies on the large size of IM domains in which the direction of the magnetization follows the RF field averaged over the volume of the domain. It implies smooth rotation of the magnetization from one domain to the other. The argument would not apply to the case in which the RF field h at each site of a 3d cubic lattice is of the order of the exchange field $6Js$ created by the neighboring spins, because it would be difficult to say without direct computation whether the effect of the RF would win over the effect of the exchange. In this connection, one should notice that by considering blocks of spins of size r satisfying $a < r < R_f$, the original problem described by the Hamiltonian (2) can be rescaled to the problem described by the same Hamiltonian with the rescaled $s_r = s(r/a)^3$, $J_r = J(a/r)^5$, and $h_r = h(a/r)^{3/2}$. This gives the same expression for the correlation length, $R_f/r = (2\pi/9)(1 - 1/n)^{-1}(6J_r s_r/h_r)^2$. For the blocks of size $r \sim R_f$ one has $h_r \sim 6J_r s_r$ in the rescaled problem. This shows that the existence of a small parameter $h/(6J)$ in the original problem with weak RF may be an illusion. The original problem with $h \ll 6Js$ is mathematically equivalent to the rescaled problem in which the local exchange field and the RF field are of the same order of magnitude. At $h \gg 6Js$ the spins obviously align with the RF, yielding the state with $m = 0$. The question, therefore, is whether decreasing h from $h \gg 6J$ would result in the bifurcation or the ground state to a non-zero m at some $h \sim 6Js$. This is suggested by Figs. 10 and 11. The answer for the ground state may depend on the number of spin components n . However, looking for the ground state in a glassy system requires a different numerical algorithm based on the global energy minimization. Whether this is worth the effort is another question.

12 Acknowledgements

This work has been supported by the Grant No. DE-FG02-93ER45487 funded by U.S. Department of Energy, Office of Science.

References

1. T. C. Proctor, D. A. Garanin, and E. M. Chudnovsky, Phys. Rev. Lett. **112**, 097201 (2014).
2. D. A. Garanin, E. M. Chudnovsky, and T. C. Proctor, Europhys. Lett. **103**, 67009 (2013).
3. D. A. Garanin, E. M. Chudnovsky, and T. Proctor, Phys. Rev. B **88**, 224418 (2013).
4. A. I. Larkin, Sov. Phys. JETP **31**, 784 (1970).
5. G. Blatter, M. V. Feigel'man, V. B. Geshkenbein, A.I. Larkin, and V. M. Vinokur, Rev. Mod. Phys. **66**, 1125 (1994).
6. Y. Imry and S.-k. Ma, Phys. Rev. Lett. **35**, 1399 (1975).
7. M. Aizenman and J. Wehr, Phys. Rev. Lett. **62**, 2503 (1989).
8. M. Aizenman and J. Wehr, Commun. Math. Phys. **130**, 489 (1990).
9. E.M. Chudnovsky and R.A. Serota, Phys. Rev. B **26**, 2697 (1982).
10. R. Pelcovits, E. Pytte, and J. Rudnick, Phys. Rev. Lett. **40**, 476 (1978).
11. J. D. Patterson, G. R. Grusalski, and D. J. Sellmyer, Phys. Rev. B **18**, 1377 (1978).
12. A. Aharony and E. Pytte, Phys. Rev. Lett. **45**, 1583 (1980).
13. D. S. Fisher, Phys. Rev. B **31**, 7233 (1985).
14. See, e.g., E. M. Chudnovsky, W. M. Saslow and R. A. Serota, Phys. Rev. B **33**, 251 (1986), and references therein.
15. S. Fishman and A. Aharony, J. Phys. C: Solid State Phys. **12**, L729 (1979).
16. K. Binder and A. P. Young, Rev. Mod. Phys. **58**, 801 (1986).
17. R. Seshadri and R.M. Westervelt, Phys. Rev. B **46**, 5142 (1992); *ibid.* **46**, 5150 (1992).
18. E. M. Chudnovsky, Phys. Rev. B **43**, 7831 (1991).
19. K. B. Efetov and A. I. Larkin, Sov. Phys. JETP **72**, 2350 (1977).
20. T. Bellini, N. A. Clark, V. Degiorgio, F. Mantegazza, and G. Natale, Phys. Rev. E **57**, 2996 (1998).
21. E. M. Chudnovsky, Phys. Rev. Lett. **103**, 137001 (2009).
22. G. E. Volovik, J. Low Temp. Phys. **150**, 453 (2008).
23. J. I. A. Li, J. Pollanen, A. M. Zimmerman, C. A. Collett, W. J. Gannon, and W. P. Halperin, Nat. Phys. **9**, 775 (2013).
24. J. L. Cardy and S. Ostlund, Phys. Rev. B **25**, 6899 (1982).
25. J. Villain and J. F. Fernandez, Z. Phys. B - Condens. Matter **54**, 139 (1984).
26. T. Nattermann, Phys. Rev. Lett. **64**, 2454 (1990).
27. J. Kierfield, T. Nattermann, and T. Hwa, Phys. Rev. B **55**, 626 (1997).
28. S. E. Korshunov, Phys. Rev. B **48**, 3969 (1993).
29. T. Giamarchi and P. Le Doussal, Phys. Rev. Lett. **72**, 1530 (1994).
30. T. Giamarchi and P. Le Doussal, Phys. Rev. B **52**, 1242 (1995).

31. See, e.g., T. Nattermann and S. Scheidl, *Adv. of Phys.* **49**, 607 (2000), and references therein.
32. D. E. Feldman, *Phys. Rev. B* **61**, 382 (2000).
33. P. Le Doussal and K. J. Wiese, *Phys. Rev. Lett.* **96**, 197202 (2006).
34. P. Le Doussal, *Phys. Rev. Lett.* **96**, 235702 (2006).
35. A. A. Middleton, P. Le Doussal, and K. J. Wiese, *Phys. Rev. Lett.* **98**, 155701 (2007).
36. S. Bogner, T. Emig, A. Taha, and C. Zeng, *Phys. Rev. B* **69**, 104420 (2004).
37. H. Orland and Y. Shapir, *Europhys. Lett.* **30**, 203 (1995).
38. T. Garel, G. Lori, and H. Orland, *Phys. Rev. B* **53**, R2941 (1996).
39. D. Fisher, *Phys. Rev. Lett.* **78**, 1964 (1997).
40. R. Dickman and E. M. Chudnovsky, *Phys. Rev. B* **44**, 4397 (1991).
41. B. Dieny and B. Barbara, *Phys. Rev. B* **41**, 11549 (1990).
42. R. Fisch, *Phys. Rev. B* **52**, 12512 (1995); *ibid* **55**, 8211 (1997); *ibid* **57**, 269 (1998); *ibid* **62**, 361 (2000); *ibid* **76**, 214435 (2007); *ibid* **79**, 214429 (2009).
43. M. J. P. Gingras and D. A. Huse, *Phys. Rev. B* **53**, 15193 (1996).
44. C. Zeng, P. L. Leath, and D. S. Fisher, *Phys. Rev. Lett.* **82**, 1935 (1999).
45. A. Perret, Z. Ristivojevic, P. Le Doussal, G. Schehr, and K. J. Wiese, *Phys. Rev. Lett.* **109**, 157205 (2012).
46. C. Zeng, A. A. Middleton, and Y. Shapir, *Phys. Rev. Lett.* **77**, 3204 (1996).
47. H. Rieger and U. Blasum, *Phys. Rev. B* **55**, R7394 (1997).
48. M. Itakura, *Phys. Rev. B* **68**, 100405(R) (2003).
49. M. Itakura and C. Arakawa, *Prog. Theor. Phys. Suppl.* No. **157**, 136 (2005).
50. T. Klein, I. Joumard, S. Blanchard, J. Marcus, R. Cubitt, T. Giamarchi, and P. Le Doussal, *Nature* **413**, 404 (2001).
51. H. E. Stanley, *Phys. Rev.* **176**, 718 (1968).
52. D. A. Garanin and H. Kachkachi, *Phys. Rev. Lett.* **90**, 65504 (2003).